Stonefish toxin defines an ancient branch of the perforin-like superfamily

Andrew M. Ellisdon[a,b], Cyril F. Reboul[a,b], Santosh Panjikar[a,c], Kitmun Huynh[a], Christine A. Oellig[a], Kelly L. Winter[a,d], Michelle A. Dunstone[a,b,e], Wayne C. Hodgson[d], Jamie Seymour[f], Peter K. Dearden[g], Rodney K. Tweten[h], James C. Whisstock[a,b,1,2], and Sheena McGowan[e,1,2]

[a]Biomedicine Discovery Institute and Department of Biochemistry and Molecular Biology, Monash University, Melbourne, VIC, 3800, Australia; [b]Australian Research Council Centre of Excellence in Advanced Molecular Imaging, Monash University, Melbourne, VIC, 3800, Australia; [c]Australian Synchrotron, Macromolecular Crystallography, Melbourne, VIC, 3168, Australia; [d]Biomedicine Discovery Institute and Department of Pharmacology, Monash University, Melbourne, VIC, 3800, Australia; [e]Biomedicine Discovery Institute and Department of Microbiology, Monash University, Melbourne, VIC, 3800, Australia; [f]Centre for Biodiscovery and Molecular Development of Therapeutics, Australian Institute of Tropical Health and Medicine, James Cook University, Cairns, QLD, 4870, Australia; [g]Department of Biochemistry and Genetics Otago, University of Otago, Dunedin, 9054 Aotearoa–New Zealand; and [h]Department of Microbiology and Immunology, University of Oklahoma Health Sciences Center, Oklahoma City, OK 73104

Edited by Brenda A. Schulman, St. Jude Children's Research Hospital, Memphis, TN, and approved November 3, 2015 (received for review April 19, 2015)

The lethal factor in stonefish venom is stonustoxin (SNTX), a heterodimeric cytolytic protein that induces cardiovascular collapse in humans and native predators. Here, using X-ray crystallography, we make the unexpected finding that SNTX is a pore-forming member of an ancient branch of the Membrane Attack Complex-Perforin/Cholesterol-Dependent Cytolysin (MACPF/CDC) superfamily. SNTX comprises two homologous subunits (α and β), each of which comprises an N-terminal pore-forming MACPF/CDC domain, a central focal adhesion-targeting domain, a thioredoxin domain, and a C-terminal tripartite motif family-like PRY SPla and the RYanodine Receptor immune recognition domain. Crucially, the structure reveals that the two MACPF domains are in complex with one another and arranged into a stable early prepore-like assembly. These data provide long sought after near-atomic resolution insights into how MACPF/CDC proteins assemble into prepores on the surface of membranes. Furthermore, our analyses reveal that SNTX-like MACPF/CDCs are distributed throughout eukaryotic life and play a broader, possibly immune-related function outside venom.

pore | stonefish | toxin | perforin | cytolysin

Human envenoming by the tropical stonefish (*Synanceia horrida* and related species) results in extreme pain, edema, hypotension, respiratory distress, and on rare occasions, death (1). The lethal factor in stonefish venom is an ∼150-kDa protein termed stonustoxin (SNTX), an unusual example of a vertebrate cytolytic protein complex (2). SNTX is a soluble heterodimeric assembly of two closely related proteins termed SNTX-α and -β that share sequence identity of ∼50% (3). With the exception of a C-terminal PRY SPla and the RYanodine Receptor (PRYSPRY) domain in each protein (4), SNTX shares no obvious sequence similarity to any structurally or functionally characterized molecule. SNTX induces species-specific hemolytic activity (2) by an apparent pore-forming mechanism (5). It induces platelet aggregation (6), and like the closely related Trachynilysin (from *Synanceia trachynis*), SNTX exhibits activity suggesting that it may function as a neurotoxin (7, 8).

Because eukaryote pore-forming toxins are relatively rare, we reasoned that SNTX might represent a new exemplar of a vertebrate pore-forming protein. Previous studies had shown that it was possible to purify and crystallize SNTX (9); however, no structure has been reported to date. Accordingly, to address the structural basis for SNTX activity, we determined its X-ray crystal structure.

Results and Discussion

SNTX Is a Heterodimer of Two Distinct Membrane Attack Complex-Perforin/Cholesterol-Dependent Cytolysin-Like Proteins. We purified SNTX from crude venom and determined its crystal structure to 3.1 Å using anomalous scattering methods (Tables S1 and S2). SNTX-α and -β form an obligate dimer with an extensive parallel interface along their entire 115-Å length (2,908 Å^2 buried surface area) (Fig. 1 *A–D* and Fig. S1). Fold recognition searches reveal that each SNTX protein comprises four domains (Fig. 1 *B* and *C*) (10). Despite a lack of obvious sequence similarity, the N-terminal domain (residues 1–265) (shown in green in Fig. 1*B*) is homologous to the Membrane Attack Complex-Perforin/Cholesterol-Dependent Cytolysin (MACPF/CDC) pore-forming domain (Fig. S2). The N-terminal MACPF/CDC domain leads into a focal adhesion-targeting (FAT) domain (266–385) (shown in dark blue in Fig. 1*B*), with highest structural similarity to the human focal adhesion kinase 1 FAT domain (rmsd of 2.7 Å over 98 aligned residues) (11). FAT domains are found in a wide range of proteins and typically perform a scaffolding role (for example, in the assembly of signaling complexes) (12). In SNTX, the FAT domain makes numerous *in cis* contacts with the MACPF/CDC domain and the thioredoxin (THX) domain (386–517) (shown in gray in Fig. 1*B* and Fig. S2) as well as extensive *in trans* interactions at the SNTX-α/β interface (Fig. S1).

The THX domain comprises a five-stranded β-sheet and shares greatest structural similarity with *Saccharomyces cerevisiae* mitochondrial THX3 (rmsd of 2.1 Å over 72 aligned residues) (13). THX domains are typically involved in redox regulation;

Significance

Here, we present the structure of the pore-forming toxin stonustoxin (SNTX), the lethal factor present in stonefish venom. Our work shows that SNTX comprises two homologous subunits (α and β), each of which belongs to the perforin superfamily of pore-forming immune effectors. In SNTX, the α- and β-Membrane Attack Complex-Perforin/Cholesterol-Dependent Cytolysin (MACPF/CDC) domains interact and form a prepore-like complex. These data provide, to our knowledge, the first high-resolution insights into how MACPF/CDCs interact with one another during pore formation.

Author contributions: J.C.W. and S.M. designed research; A.M.E., C.F.R., S.P., K.H., C.A.O., K.L.W., J.S., P.K.D., R.K.T., and S.M. performed research; K.L.W., W.C.H., J.S., and S.M. contributed new reagents/analytic tools; A.M.E., C.F.R., M.A.D., P.K.D., R.K.T., J.C.W., and S.M. analyzed data; and A.M.E., J.C.W., and S.M. wrote the paper.

The authors declare no conflict of interest.

This article is a PNAS Direct Submission.

Data deposition: Crystallography, atomic coordinates, and structure factors have been deposited in the Protein Data Bank, www.pdb.org (PDB ID code 4WVM).

[1]J.C.W. and S.M. contributed equally to this work.

[2]To whom correspondence may be addressed. Email: James.Whisstock@monash.edu or sheena.mcgowan@monash.edu.

This article contains supporting information online at www.pnas.org/lookup/suppl/doi:10.1073/pnas.1507622112/-/DCSupplemental.

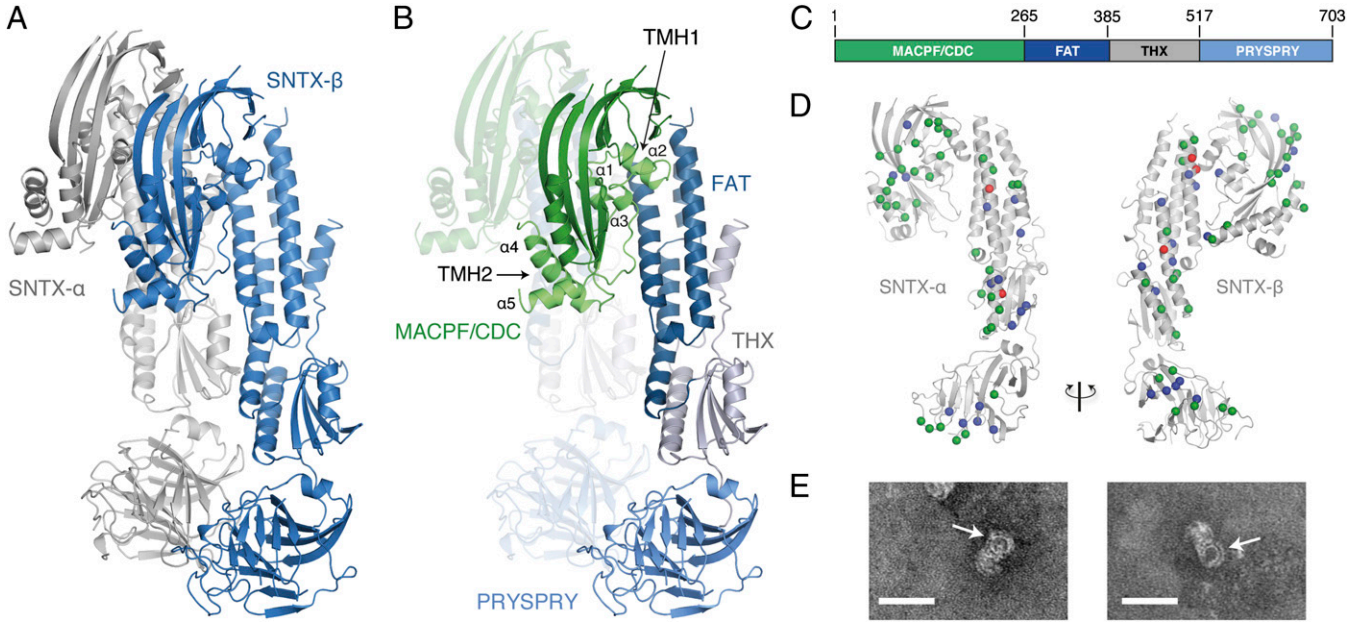

Fig. 1. The SNTX structure reveals an MACPF/CDC pore-forming heterodimer. (*A*) Crystal structure of the SNTX heterodimer with SNTX-α (gray) and SNTX-β (blue) shown in cartoon format. (*B*) The SNTX-domain layout in cartoon format and schematic representation. (*C*) Schematic representation of the SNTX domain layout. (*D*) The interaction interface between each SNTX subunit. The Cα-atoms of the interacting residues are colored as per the interaction type, with salt bridges in red, hydrogen bonds in blue, and buried hydrophobics (>20 Å^2 buried surface area) in green. Interacting residues were calculated by PISA (57). (*E*) Transmission EM of SNTX pores that are indicated by arrows. (Scale bar: 50 nm.)

however, the SNTX THX domain lacks the canonical catalytic residues (Fig. S2). We, therefore, suggest that, in SNTX, the THX domain may play a purely structural role.

Finally, the PRYSPRY domains (518–703) (shown in blue in Fig. 1*B*) of each subunit interact in the heterodimer and are located distal to the MACPF/CDC domain. The PRYSPRY

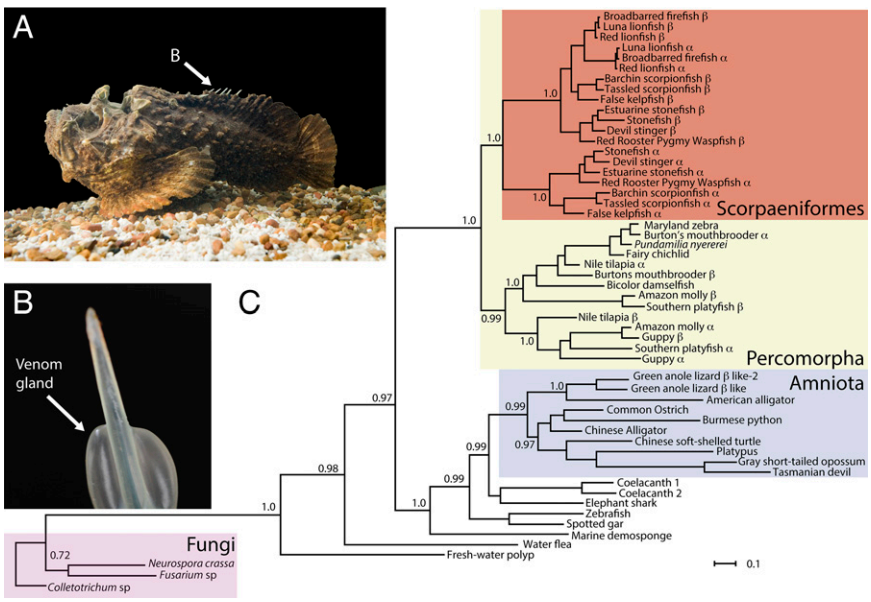

Fig. 2. SNTX-like proteins form an extensive and ancient third branch of the MACPF/CDC superfamily. (*A*) The tropical stonefish (*S. horrida*) highlighting 13 dorsal spines that deliver venom. (*B*) Close-up view of the venom glands located on either side of a dorsal spine. (*C*) Rooted Bayesian phylogram of SNTX-like protein sequences from animals and fungi. SNTX-like proteins are defined as proteins sharing significant sequence identity in the SNTX MACPF/CDC domain. Node labels indicate posterior probabilities. The α- and β-subunit sequences are very similar, and the phylogeny indicates that different subunits have evolved multiple times, probably through gene duplication and perhaps, gene conversion. The SNTX-like proteins from venomous species of fish form a sister clade to those from closely related fish groups. Branch lengths in this region of the tree indicate that SNTX-like proteins used as venoms do not vary hugely from those in nonvenomous fish. As such, use of these proteins as toxins may have more to do with expression levels and location than significant evolutionary change. SNTX-like proteins are found in a variety of vertebrates, including the common ostrich, platypus, Tasmanian devil, and coelacanth. The presence of an SNTX-like protein in a member of the Porifera [*Amphemidon* (Demosponge)] implies that SNTX-like proteins predate the evolution of metazoa. The fact that similar SNTX MACPF/CDC domain proteins are found in fungi implies that this molecule predates animals and was, therefore, present in the ancestors of fungi and animals.

domains share greatest structural similarity to the tripartite motif family (TRIM) 21 PRYSPRY domain (rmsd of 1.55 Å over 155 aligned residues) that participates in immune recognition of intracellular bacteria and viruses (14, 15).

The presence of an MACPF/CDC domain in SNTX immediately suggested a mechanism of stonefish venom toxicity (Fig. 2 *A* and *B*). MACPF/CDC proteins typically form large, ring-shaped supramolecular oligomeric pore complexes in membranes. Accordingly, using transmission EM, we observed that SNTX forms large ring-shaped pores in rat erythrocyte membranes (Fig. 1*E* and Fig. S3). These images provide the first direct evidence, to our knowledge, of SNTX pore formation. The pores had an outer dimension of 257 ± 5.7 Å (mean ± SEM) and a lumen i.d. of 117 ± 4.5 Å. These data together establish SNTX as a bona fide pore-forming member of the MACPF/CDC superfamily.

CDCs were originally identified as pore-forming toxins found in pathogenic Gram-positive bacteria (16). Despite little primary sequence identity, subsequent structural studies revealed that MACPF proteins, such as the mammalian immune pore-forming proteins perforin and the terminal components of complement, were homologous to CDCs (17, 18). Database searches and phylogenetic studies reveal that MACPFs and CDCs can be found throughout life and represent two major branches of a pore-forming toxin superfamily that diverged from an ancient common ancestor (18). The core conserved MACPF/CDC fold is a four-stranded, highly twisted, antiparallel β-sheet against which pack two bundles of α-helices [transmembrane helix 1 (TMH1) and TMH2] (Fig. 1*B*). During pore formation, the MACPF/CDC domain self-associates to form an early prepore. Subsequently, the central β-sheet substantially untwists, and both TMH1 and TMH2 unwind to form the β-strands of the final β-barrel pore (Fig. S4) (19–23). However, our current molecular understanding of pore assembly is severely limited by a lack of any high-resolution structural examples of MACPF/CDC pores or assembly intermediates in a pore-compatible conformation.

Both SNTX Subunits Contain a Minimal MACPF/CDC Pore-Forming Domain Together with a PRYSPRY Domain That Likely Mediates Binding to the Cell Surface. Structural comparisons reveal that the two SNTX MACPF/CDC domains are substantially pared down compared with other structurally characterized family members and essentially, comprise the core pore-forming machinery (i.e., the four-stranded β-sheet together with TMH1 and TMH2) (Fig. 1*B*). These data also suggest that the SNTX MACPF/CDC domain more closely resembles the CDCs rather than MACPF proteins (Fig. S2). In contrast, structure-guided sequence alignments revealed that the highly conserved MACPF signature motif, which is absent in CDCs, is present in SNTX-like proteins (Fig. S2) (18). Together, these observations suggest that, although SNTX-like proteins represent an extremely early divergence from the MACPF branch of the superfamily, they still retain significant CDC-like characteristics.

MACPF/CDC proteins use different mechanisms to initially interact with the membrane. For example, in CDCs, membrane binding is mediated through an Ig-like "domain 4" (16, 24, 25), whereas perforin deploys a C-terminal lipid binding C2 domain (21). In SNTX, the pair of PRYSPRY domains is located in an analogous position to the Ig and C2 domains of CDCs and perforin, respectively. PRYSPRY domains mediate protein–protein and protein–lipid interactions, particularly in the context of pathogen recognition in TRIM immune proteins (26). Accordingly, it is anticipated that the PRYSPRY domain of both SNTX subunits would be responsible for initial interaction with the cell surface through either lipid- or protein-mediated interactions. Consistent with this idea, the canonical protein/lipid binding pocket of each PRYSPRY domain (27) is located at the solvent-exposed base of each SNTX molecule (Fig. 3*A*). By analogy with other MACPF/CDC proteins, such a binding mode would position the SNTX MACPF/CDC domains appropriately for pore assembly.

Phylogenetic Analysis Reveals That SNTX Represents an Ancient Third Branch of the MACPF/CDC Superfamily. We next explored the distribution of SNTX-like proteins throughout life. Sequence and phylogenetic studies reveal that SNTX-like proteins can be readily identified (over 50 proteins) in a wide range of venomous and nonvenomous fish, reptiles, birds, monotreme mammals, a water flea, a marine sponge, and certain fungi (Fig. 2*C* and Dataset S1). Despite this broad distribution, SNTX-like proteins were not detected in some major groups, such as the *Lophotrochozoa* or nematodes. Together, this distribution suggests a deep evolutionary history for these genes, with considerable gene loss evident in multiple branches. The genomes of many ancient eukaryotes that contain SNTX-like genes also have readily identifiable MACPF-like proteins, such as Macrophage Perforin-like Encoded Gene-1 (28, 29). Therefore, SNTX-like proteins represent an extensive and ancient third branch of the MACPF/CDC superfamily.

Our phylogenetic analyses also imply that SNTX-α and -β were generated by gene duplication multiple times throughout the evolutionary history of Percomorpha fish (Fig. 2*C*). This finding contrasts with the single SNTX-like monomer encoded in the genomes of non-Percomorphic fish and other animals. It, thus, seems likely that SNTX-α and -β arose through gene duplication of this ancestral monomeric pore-forming SNTX-like protein.

Crystal Structure of the SNTX Heterodimer Presents a Soluble Exemplar of an MACPF/CDC Prepore-Like Complex. Extensive published experimental data reveal that a key step in prepore assembly is formation of a stable membrane-bound dimer (30). We suggest that the structure of the SNTX heterodimer represents a soluble and stable snapshot of this event. Consistent with this idea, the orientation of the two MACPF/CDC domains in the SNTX heterodimer resembles the arrangement of MACPF/CDC domains seen in low-resolution EM structures (>15 Å) of MACPF/CDC prepore assemblies (22, 23, 31). Furthermore, our phylogenetic data suggest that, after duplication, SNTX-α and -β initially functioned as monomers but then, coevolved to function as a stable dimer.

Within the SNTX-α/β MACPF/CDC domain interface, the two central twisted β-sheets abut with strand-β4 of SNTX-α and strand-β1 of SNTX-β, forming bona fide β-sheet hydrogen bonds (Fig. 3*B*). Although this feature has not been previously observed at high resolution, these data are in agreement with the long-held idea that formation of a giant and continuous β-sheet between subunits at the rim of the nascent prepore is an important part of the initial assembly mechanism (32).

Farther down the sheet, the β4- and β1-strands splay apart from one another. The base of the splayed β-strands are linked by a long-range ion pair between K205 in SNTX-α strand-β4 and E55 in SNTX-β strand-β1 (Fig. 3*D*). This structure can, thus, be considered analogous to a partly closed zipper. Previously, for MACPF and CDCs, it has been suggested that polar interactions between the β4- and β1-strands in the prepore function to pull the strands together during formation of the full β-barrel pore (23). Finally, analysis of the general surface charge at the SNTX dimer interface reveals that the charge distribution of each face is largely complementary, with the α-subunit interface positively charged and the β-subunit interface negatively charged (Fig. S1). These data are consistent with suggestions that charge complementarity between perforin monomers may drive initial oligomerization events (33, 34).

Structural Analysis of the SNTX Dimer in the Context of a Full Prepore Model Provides Broad Mechanistic Insight into Prepore Assembly. Based on the EM structures of both MACPF proteins and CDCs, additional oligomerization events predictably require an

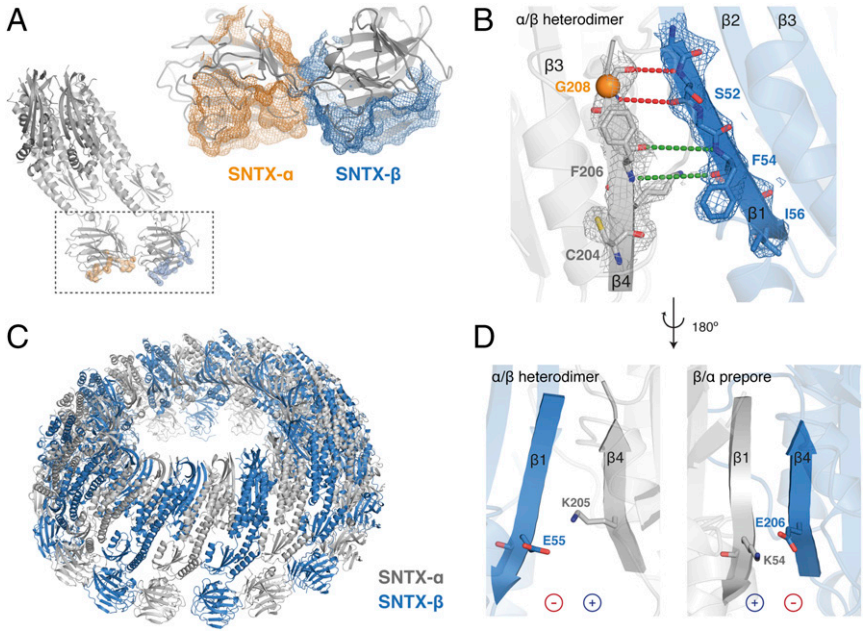

Fig. 3. Structural basis of SNTX membrane binding and prepore assembly. (*A*) The PRYSPRY protein/lipid binding pocket is shown as Cα-atom spheres on SNTX-α (orange) and SNTX-β (blue). Residues in the protein/lipid-binding pocket were located by structural alignment [PDBeFold (57)] with the TRIM21:IgG-Fc complex [Protein Data Bank ID code 2IWG (58)]. SNTX PRYSPRY domain residues aligning with the TRIM21 residues that make significant contacts with IgG-Fc are highlighted. The binding pocket is also represented as surface mesh on a zoomed in orientation of the PRYSPRY dimer. (*B*) The SNTX MACPF/CDC interface within the heterodimer. Hydrogen bonds between strand-β4 of SNTX-α and strand-β1 of SNTX-β are highlighted as red dashed lines, and aligned residues are indicated by green dashed lines. The β-strands are numbered according to their position in the MACPF/CDC central β-sheet. The conserved G208 residue is shown as a sphere at the Cα-atom position, and the electron density difference (2Fo-Fc) map is contoured at 1σ. (*C*) The SNTX prepore model calculated by extrapolation of 18° of internal symmetry between SNTX subunits. (*D*) Close-up view of the MACPF/CDC electrostatic interaction at the α/β-heterodimer interface and the β/α-prepore interface (59, 60).

SNTX-α/β heterodimer to form a β/α-interface with a partner SNTX molecule. Using the SymD algorithm (35) and CE-Symm (36), we determined that each SNTX subunit is related by 18° of internal rotational symmetry (i.e., the number of degrees of rotation that would be required to transpose one SNTX subunit so that it completely aligns to the second subunit) (Fig. S5). Full extrapolation of this symmetry allows us to build a model of a complete early prepore assembly (i.e., before β-sheet opening). With the symmetry axis positioned at the center of the prepore assembly, the final prepore consists of 20 SNTX subunits and thus, has 20-fold rotational symmetry (C_{20}) (Fig. S5). Therefore, the prepore model is composed of 10 SNTX-α/β heterodimers that align along a horizontal plane (Fig. 3*C*). The model has an o.d. of 259 Å and a lumen i.d. of 112 Å (in close agreement with our EM images of SNTX pores) (Fig. 1*E* and Fig. S5).

The interface between SNTX-β and -α formed in the prepore model shares, as expected, many of the features already described for the SNTX-α/β heterodimer. For example, as seen in the heterodimer structure, we predict that the molecules will assemble such that a continuous antiparallel β-sheet runs around the rim of the prepore (Fig. 3*C* and Fig. S5). Similarly, our model suggests that oligomerization of SNTX is driven by complementary charges on the interacting surfaces. Crucially, it is suggested that the polar interactions are maintained at the newly formed interface between SNTX-α strand-β1 and SNTX-β strand-β4. In this interface, however, we predict that charges are reversed, such that SNTX-β E206 on strand-β4 forms a likely long-range ion pair to SNTX-α K54 on strand-β1 (Fig. 3*D*).

Importantly, the prepore model reveals remarkably few steric clashes between SNTX heterodimers. Indeed, our data suggest that the only significant structural change that must take place to permit addition of further SNTX heterodimers is rearrangement of the interface between the β4-α6 loop in SNTX-β and the SNTX-α TMH2/helix-α6 against which it abuts (Fig. S5).

Within the SNTX heterodimer, the SNTX-α β4-α6 loop locks into a hydrophobic surface pocket of SNTX-β that is formed by TMH2, helix-α6, and strand-β1 (Fig. S5*C*) (termed the β4-α6 binding site). During oligomerization, it is, therefore, anticipated that the SNTX-β β4-α6 loop of one STNX protein must move to lock into the β4-α6 binding site of an incoming SNTX-α subunit present in the adjacent molecule (Fig. S5*D*). Crucially and consistent with this idea, mutagenesis of the equivalent β4-α6 loop structure in CDCs (the β5-region) showed that mobility in this region is essential for initial stable dimer formation as well as subsequent oligomerization events (30, 32). Similarly, EM data and mutagenesis data suggest that the equivalent region is also important for assembly of the fungal MACPF protein pleurotolysin (23). Taken together, our data on SNTX suggest that the region equivalent to the β4-α6 loop structure in MACPF and CDCs represents a key and conserved feature that is critical for initial prepore assembly.

Conclusions

Many of the toxic physiological effects of stonefish (*S. horrida* and related species) envenomation can be attributed to SNTX or related proteins (i.e., Trachynilysin from *S. trachynis*). These symptoms include endothelium-dependent vasorelaxation, hemolytic activity, edema, increases in vascular permeability, myotoxic effects on the neuromuscular junction, and severe pain (1, 3). By revealing that SNTX and related proteins are pore-forming proteins of the MACPF/CDC superfamily, our data provide the structural and molecular context for the unique physiological effects of stonefish envenomation. Many members of the MACPF/CDC superfamily possess apparently promiscuous activity against a wide range of cell types. Indeed, we suggest that SNTX may be able to form pores in cells from a

variety of target tissues, thus rationalizing the diversity of physiological consequences that arise from envenomation.

On envenomation, our data suggest that SNTX molecules would bind and assemble on target membranes to form membrane-penetrating pores. The formation of MACPF/CDC-like pores by SNTX would be central to the toxin's hemolytic activity, and cell lysis could explain physiological effects, including edema, increased vascular permeability, and muscle damage. Moreover, electrophysiological studies of the related Trachynilysin protein show a sustained increase in membrane conductance and continuous neurotransmitter release from large dense core vesicles (8, 37). Such events could also explain the endothelium-dependent vasorelaxation and the symptoms of severe pain that occur in response to stonefish envenomation. Taken together, these data are consistent with the irreversible formation of large ion-permeable transmembrane SNTX pores (38). Finally, we suggest that the recognition that SNTX-like proteins contain MACPF/CDC pore-forming domains provides a platform for future studies into the mechanism of other SNTX-like proteins found in the venoms of related fish species and other vertebrates.

Collectively, these sequence, structural, and phylogenetic analyses reveal that SNTX is representative of a third major branch of the MACPF/CDC superfamily. Consistent with an early divergence of each group, SNTX displays certain features that are more MACPF-like and others that are more reminiscent of the CDCs. Together and despite the substantial evolutionary distance between SNTX-like, CDC-like, and MACPF-like proteins, our data suggest that remarkable commonalities in mechanism likely exist across the three branches of the family.

Finally, because many SNTX-like proteins are found in nonvenomous organisms, is there a possible ancestral role of an SNTX-like protein? These data as well as the extensive distribution of SNTX-like proteins throughout life suggest that an ancestral role for SNTX is outside venom. Indeed, the presence in SNTX of a TRIM-like PRYSPRY immune recognition domain, closely related to the fish intracellular TRIM group of antiviral proteins (39), suggests a possible immune role for an ancestral SNTX-like protein (40).

Materials and Methods

Ethics Statement. Animal procedures were approved by the James Cook University Animal Ethics Committee (Ethics Approval Number A1570) and comply with the Australian Code of Practice for the Care and Use of Animals for Scientific Purposes, and the Queensland Animal Care and Protection Act 2001.

Protein Purification. SNTX was purified from venom obtained from *S. horrida* by extraction from venom glands located on either side of 13 dorsal spines. Purification of SNTX from crude venom is described in *SI Materials and Methods*. SNTX was concentrated to 5–10 mg/mL for crystallography. The activity of the purified SNTX was confirmed by a doubling dilution hemolysin assay using 1% (vol/vol) rat erythrocytes as described previously (41). The titer was defined as the reciprocal of the last well that showed complete hemolysis [$\log_2$(hemolytic activity)] and shown to be 8.25 $\pm$ 0.4 (compared with crude venom: 5.8 $\pm$ 0.3).

Structural Biology Methods. SNTX crystals were grown as described previously (9) at 20 °C by hanging drop vapor diffusion in 4–4.4 M NaCl at a protein concentration of between 5 and 10 mg/mL. SNTX crystals in mother liquor were flash-cooled in liquid nitrogen before the collection of crystallographic data at the MX2 Beamline of the Australian Synchrotron. SNTX crystals were derivatized with xenon (42) and tantalum bromide as described in *SI Materials and Methods*. The data collection protocol is also described in *SI Materials and Methods*.

Each dataset was integrated using XDS and scaled using XSCALE (43). The two sets of xenon-derivative data were merged together to improve redundancy. Anomalous signal from either of the derivatives was not sufficient to determine the substructure. Analysis of the cross-*R* factor between the native and the two derivatives indicated that native crystals were nonisomorphous with respect to each of the derivatives. However, the cross-*R* factor between the derivatives was 18%, indicating somewhat isomorphous data. Initial experimental phasing was performed using the SIRAS phasing protocol of Auto-Rickshaw (44) by treating the tantalum bromide derivative dataset as a native and the xenon dataset as a derivative.

Heavy-atom site determination, phase calculation, solvent flattening, and partial model building were performed automatically by SHELXD (45), BP3 (46), PIRATE (47), and BUCCANEER (48) within the Auto-Rickshaw software pipeline. The resulting electron density showed some interpretability for a small number of α-helices. Additional phase improvement was achieved using the MRSAD protocol of Auto-Rickshaw (49), and 40% of the model was built automatically. The model was then extended to ∼70% of the total number of residues by manual building into the resulting electron density map using COOT (50).

At this stage, the resultant phases were transferred to the native dataset and extended to 3.10-Å resolution using DMMULTI (51) by the multiple crystal averaging technique. The improved electron density map enabled building of up to 80% of the model. Finally, iterative cycles of refinement were carried out using BUSTER (52) with local rebuilding in COOT, resulting in a model with an *R* factor of 20.71% (R_{free} of 23.64%) and good geometry (Tables S1 and S2). The structure had a final MolProbity (53) score of 1.91 (100th percentile). Structural analysis and modeling are described in *SI Materials and Methods*.

EM. Transmission EM images were obtained using a Hitachi Electron Microscope with an accelerating voltage of 80 kV. Purified SNTX was incubated with 1% rat erythrocytes in PBS at 20 °C for 20 min, after which samples were adsorbed onto a carbon-coated grid and stained with 1% (wt/vol) uranyl-acetate. Rat erythrocytes lysed in water were used as negative controls.

Phylogeny. SNTX-like MACPF/CDC domain protein sequences were aligned using CLC Genomics Workbench. Consensus phylogenetic relationships were calculated using MrBayes (54) and the WAG model of protein evolution (55), which was identified as the most appropriate model after testing with mixed models. Monte Carlo Markov chains were run for 1 million generations, and the initial 25% of trees were discarded as burn in. Phylograms were visualized using Dendroscope (56). Phylogenetic trees were generated for both the whole-protein sequences and the MACPF/CDC-like domains. There is little difference between the trees, suggesting that the phylogenetic relationship is driven by the MACPF/CDC motif alone and not the rest of the primary sequence. This finding is also supported by the fact that attempts to align the proteins in the absence of the MACPF/CDC domain and produce a maximum parsimony phylogenetic tree failed using Mega6.

ACKNOWLEDGMENTS. We thank the Australian Synchrotron for beam access and technical assistance. We also thank TinaMarie Lieu and Claudia McCarthy for rat erythrocytes for cell lysis assays and transmission EM and Michelle L. Halls for critical review of the manuscript. We further thank the Monash platforms [Protein Crystallography Unit, eResearch (MASSIVE), and Biological Electron Microscopy] for technical support. C.F.R. is supported by Monash University FMNHS Bridging Postdoctoral Fellowship Award. This research was supported by an award from the National Health and Medical Research Council of Australia (NMHRC) Dora Lush Postgraduate Research Scholarship (to K.L.W.), NIH Grant 1R01 AI037657 (to R.K.T.), an ARC Federation Fellowship (to J.C.W.), and ARC Future Fellowship FT100100690 (to S.M.). Additionally, M.A.D. is an NHMRC Career Development Fellow, and J.C.W. is an NMHRC Senior Principal Research Fellow.

1. Halstead BW (1970) *Poisonous and Venomous Marine Animals of the World* (United States Government Printing Office, Washington, DC).
2. Poh C, et al. (1991) Purification and partial characterisation of stonustoxin (lethal factor) from *Synanceja horrida* venom. *Comp Biochem Physiol B* 99(4):793–798.
3. Ghadessy FJ, et al. (1996) Stonustoxin is a novel lethal factor from stonefish (*Synanceja horrida*) venom. cDNA cloning and characterization. *J Biol Chem* 271(41):25575–25581.
4. Henry J, Ribouchon M-T, Offer C, Pontarotti P (1997) B30.2-like domain proteins: A growing family. *Biochem Biophys Res Commun* 235(1):162–165.
5. Chen D, Kini RM, Yuen R, Khoo HE (1997) Haemolytic activity of stonustoxin from stonefish (*Synanceja horrida*) venom: Pore formation and the role of cationic amino acid residues. *Biochem J* 325(Pt 3):685–691.
6. Khoo HE, Yuen R, Poh CH, Tan CH (1992) Biological activities of Synanceja horrida (stonefish) venom. *Nat Toxins* 1(1):54–60.
7. Low KS, Gwee MC, Yuen R, Gopalakrishnakone P, Khoo HE (1994) Stonustoxin: Effects on neuromuscular function in vitro and in vivo. *Toxicon* 32(5):573–581.
8. Meunier FA, et al. (2000) Trachynilysin mediates SNARE-dependent release of catecholamines from chromaffin cells via external and stored Ca2+. *J Cell Sci* 113(Pt 7):1119–1125.
9. Yew WS, Kolatkar PR, Kuhn P, Khoo HE (1999) Crystallization and preliminary crystallographic study of stonustoxin, a protein lethal factor isolated from the stonefish (Synanceja horrida) venom. *J Struct Biol* 128(2):216–218.
10. Holm L, Rosenström P (2010) Dali server: Conservation mapping in 3D. *Nucleic Acids Res* 38(Web Server issue):W545–W549.

11. Garron ML, et al. (2008) Structural basis for the interaction between focal adhesion kinase and CD4. *J Mol Biol* 375(5):1320–1328.
12. Hayashi I, Vuori K, Liddington RC (2002) The focal adhesion targeting (FAT) region of focal adhesion kinase is a four-helix bundle that binds paxillin. *Nat Struct Biol* 9(2): 101–106.
13. Bao R, Zhang Y, Zhou CZ, Chen Y (2009) Structural and mechanistic analyses of yeast mitochondrial thioredoxin Trx3 reveal putative function of its additional cysteine residues. *Biochim Biophys Acta* 1794(4):716–721.
14. Keeble AH, Khan Z, Forster A, James LC (2008) TRIM21 is an IgG receptor that is structurally, thermodynamically, and kinetically conserved. *Proc Natl Acad Sci USA* 105(16):6045–6050.
15. Mallery DL, et al. (2010) Antibodies mediate intracellular immunity through tripartite motif-containing 21 (TRIM21). *Proc Natl Acad Sci USA* 107(46):19985–19990.
16. Rossjohn J, Feil SC, McKinstry WJ, Tweten RK, Parker MW (1997) Structure of a cholesterol-binding, thiol-activated cytolysin and a model of its membrane form. *Cell* 89(5):685–692.
17. Hadders MA, Beringer DX, Gros P (2007) Structure of C8alpha-MACPF reveals mechanism of membrane attack in complement immune defense. *Science* 317(5844): 1552–1554.
18. Rosado CJ, et al. (2007) A common fold mediates vertebrate defense and bacterial attack. *Science* 317(5844):1548–1551.
19. Shatursky O, et al. (1999) The mechanism of membrane insertion for a cholesterol-dependent cytolysin: A novel paradigm for pore-forming toxins. *Cell* 99(3):293–299.
20. Shepard LA, et al. (1998) Identification of a membrane-spanning domain of the thiol-activated pore-forming toxin Clostridium perfringens perfringolysin O: An alpha-helical to beta-sheet transition identified by fluorescence spectroscopy. *Biochemistry* 37(41):14563–14574.
21. Law RHP, et al. (2010) The structural basis for membrane binding and pore formation by lymphocyte perforin. *Nature* 468(7322):447–451.
22. Tilley SJ, Orlova EV, Gilbert RJC, Andrew PW, Saibil HR (2005) Structural basis of pore formation by the bacterial toxin pneumolysin. *Cell* 121(2):247–256.
23. Lukoyanova N, et al. (2015) Conformational changes during pore formation by the perforin-related protein pleurotolysin. *PLoS Biol* 13(2):e1002049.
24. Farrand AJ, LaChapelle S, Hotze EM, Johnson AE, Tweten RK (2010) Only two amino acids are essential for cytolytic toxin recognition of cholesterol at the membrane surface. *Proc Natl Acad Sci USA* 107(9):4341–4346.
25. Ramachandran R, Heuck AP, Tweten RK, Johnson AE (2002) Structural insights into the membrane-anchoring mechanism of a cholesterol-dependent cytolysin. *Nat Struct Biol* 9(11):823–827.
26. Ozato K, Shin DM, Chang TH, Morse HC, 3rd (2008) TRIM family proteins and their emerging roles in innate immunity. *Nat Rev Immunol* 8(11):849–860.
27. Sebastian S, et al. (2009) An invariant surface patch on the TRIM5alpha PRYSPRY domain is required for retroviral restriction but dispensable for capsid binding. *J Virol* 83(7):3365–3373.
28. D'Angelo ME, Dunstone MA, Whisstock JC, Trapani JA, Bird PI (2012) Perforin evolved from a gene duplication of MPEG1, followed by a complex pattern of gene gain and loss within Euteleostomi. *BMC Evol Biol* 12:59.
29. Wiens M, et al. (2005) Innate immune defense of the sponge Suberites domuncula against bacteria involves a MyD88-dependent signaling pathway. Induction of a perforin-like molecule. *J Biol Chem* 280(30):27949–27959.
30. Hotze EM, et al. (2012) Monomer-monomer interactions propagate structural transitions necessary for pore formation by the cholesterol-dependent cytolysins. *J Biol Chem* 287(29):24534–24543.
31. Leung C, et al. (2014) Stepwise visualization of membrane pore formation by suilysin, a bacterial cholesterol-dependent cytolysin. *eLife* 3:e04247.
32. Ramachandran R, Tweten RK, Johnson AE (2004) Membrane-dependent conformational changes initiate cholesterol-dependent cytolysin oligomerization and intersubunit beta-strand alignment. *Nat Struct Mol Biol* 11(8):697–705.
33. Baran K, et al. (2009) The molecular basis for perforin oligomerization and transmembrane pore assembly. *Immunity* 30(5):684–695.
34. Köster S, et al. (2014) Crystal structure of listeriolysin O reveals molecular details of oligomerization and pore formation. *Nat Commun* 5:3690.
35. Tai CH, Paul R, Dukka KC, Shilling JD, Lee B (2014) SymD webserver: A platform for detecting internally symmetric protein structures. *Nucleic Acids Res* 42(Web Server issue):W296–W300.
36. Myers-Turnbull D, et al. (2014) Systematic detection of internal symmetry in proteins using CE-Symm. *J Mol Biol* 426(11):2255–2268.
37. Ouanounou G, Malo M, Stinnakre J, Kreger AS, Molgo J (2002) Trachynilysin, a neurosecretory protein isolated from stonefish (Synanceia trachynis) venom, forms nonselective pores in the membrane of NG108-15 cells. *J Biol Chem* 277(42): 39119–39127.
38. Sung JM, Low KS, Khoo HE (2002) Characterization of the mechanism underlying stonustoxin-mediated relaxant response in the rat aorta in vitro. *Biochem Pharmacol* 63(6):1113–1118.
39. van der Aa LM, et al. (2009) A large new subset of TRIM genes highly diversified by duplication and positive selection in teleost fish. *BMC Biol* 7:7.
40. Buchmann K (2014) Evolution of innate immunity: Clues from invertebrates via fish to mammals. *Front Immunol* 5(5):459.
41. Awad MM, Bryant AE, Stevens DL, Rood JI (1995) Virulence studies on chromosomal alpha-toxin and theta-toxin mutants constructed by allelic exchange provide genetic evidence for the essential role of alpha-toxin in *Clostridium perfringens*-mediated gas gangrene. *Mol Microbiol* 15(2):191–202.
42. Panjikar S, Tucker PA (2002) Xenon derivatization of halide-soaked protein crystals. *Acta Crystallogr D Biol Crystallogr* 58(Pt 9):1413–1420.
43. Kabsch W (2010) XDS. *Acta Crystallogr D Biol Crystallogr* 66(Pt 2):125–132.
44. Panjikar S, Parthasarathy V, Lamzin VS, Weiss MS, Tucker PA (2005) Auto-rickshaw: An automated crystal structure determination platform as an efficient tool for the validation of an X-ray diffraction experiment. *Acta Crystallogr D Biol Crystallogr* 61(Pt 4): 449–457.
45. Schneider TR, Sheldrick GM (2002) Substructure solution with SHELXD. *Acta Crystallogr D Biol Crystallogr* 58(Pt 10 Pt 2):1772–1779.
46. Pannu NS, Read RJ (2004) The application of multivariate statistical techniques improves single-wavelength anomalous diffraction phasing. *Acta Crystallogr D Biol Crystallogr* 60(Pt 1):22–27.
47. Cowtan K (2000) General quadratic functions in real and reciprocal space and their application to likelihood phasing. *Acta Crystallogr D Biol Crystallogr* 56(Pt 12): 1612–1621.
48. Cowtan K (2006) The Buccaneer software for automated model building. 1. Tracing protein chains. *Acta Crystallogr D Biol Crystallogr* 62(Pt 9):1002–1011.
49. Panjikar S, Parthasarathy V, Lamzin VS, Weiss MS, Tucker PA (2009) On the combination of molecular replacement and single-wavelength anomalous diffraction phasing for automated structure determination. *Acta Crystallogr D Biol Crystallogr* 65(Pt 10):1089–1097.
50. Emsley P, Cowtan K (2004) Coot: Model-building tools for molecular graphics. *Acta Crystallogr D Biol Crystallogr* 60(Pt 12 Pt 1):2126–2132.
51. Collaborative Computational Project, Number 4 (1994) The CCP4 suite: Programs for protein crystallography. *Acta Crystallogr D Biol Crystallogr* 50(Pt 5):760–763.
52. Bricogne G, et al. (2011) *BUSTER Version 2.11.2* (Global Phasing Ltd., Cambridge, United Kingdom).
53. Chen VB, et al. (2010) MolProbity: All-atom structure validation for macromolecular crystallography. *Acta Crystallogr D Biol Crystallogr* 66(Pt 1):12–21.
54. Ronquist F, Huelsenbeck JP (2003) MrBayes 3: Bayesian phylogenetic inference under mixed models. *Bioinformatics* 19(12):1572–1574.
55. Whelan S, Goldman N (2001) A general empirical model of protein evolution derived from multiple protein families using a maximum-likelihood approach. *Mol Biol Evol* 18(5):691–699.
56. Huson DH, et al. (2007) Dendroscope: An interactive viewer for large phylogenetic trees. *BMC Bioinformatics* 8:460.
57. Krissinel E, Henrick K (2007) Inference of macromolecular assemblies from crystalline state. *J Mol Biol* 372(3):774–797.
58. James LC, Keeble AH, Khan Z, Rhodes DA, Trowsdale J (2007) Structural basis for PRYSPRY-mediated tripartite motif (TRIM) protein function. *Proc Natl Acad Sci USA* 104(15):6200–6205.
59. Reboul CF, Mahmood K, Whisstock JC, Dunstone MA (2012) Predicting giant transmembrane β-barrel architecture. *Bioinformatics* 28(10):1299–1302.
60. Sato TK, Tweten RK, Johnson AE (2013) Disulfide-bond scanning reveals assembly state and β-strand tilt angle of the PFO β-barrel. *Nat Chem Biol* 9(6):383–389.
61. Kabsch W, Sander C (1983) Dictionary of protein secondary structure: Pattern recognition of hydrogen-bonded and geometrical features. *Biopolymers* 22(12): 2577–2637.
62. Konagurthu AS, et al. (2010) MUSTANG-MR structural sieving server: Applications in protein structural analysis and crystallography. *PLoS One* 5(4):e10048.
63. Potterton L, et al. (2004) Developments in the CCP4 molecular-graphics project. *Acta Crystallogr D Biol Crystallogr* 60(Pt 12 Pt 1):2288–2294.
64. Ashkenazy H, Erez E, Martz E, Pupko T, Ben-Tal N (2010) ConSurf 2010: Calculating evolutionary conservation in sequence and structure of proteins and nucleic acids. *Nucleic Acids Res* 38(Web Server issue):W529–W533.
65. Lovelace LL, Cooper CL, Sodetz JM, Lebioda L (2011) Structure of human C8 protein provides mechanistic insight into membrane pore formation by complement. *J Biol Chem* 286(20):17585–17592.